Proceedings of the ASME/BATH 2023
Symposium on Fluid Power and Motion Control
FPMC2023
October 16-18, 2023, Sarasota, FL, USA

FPMC2023-111497

CONTROL OF HYDRAULIC INJECTION MOULDING MACHINE WITH ELECTRO-HYDRAULIC VARIABLE-SPEED DRIVE

Rasmus A. Hertz[1,*], Ole Therkelsen[1], Søren Kristiansen[2], Jesper K. Christensen[3], Frederik A. Hansson[4], Lasse Schmidt [4]

[1]R&D Moulding, LEGO System A/S
[2]Materials Department, LEGO System A/S
[3]Moulding Analytics Center, LEGO System A/S
[4]AAU Energy, Aalborg University

ABSTRACT

In this work an industrial hydraulic injection moulding machine, is retrofitted with a electro-hydraulic variable-speed drive. The focus is placed on the injection cylinder, where the design of the hydraulic system is realized with standard components. The design is based on two permanent magnet synchronous motors connected to two fixed displacement pumps, allowing the control of the injection cylinder without the need for valves in the flow path, removing the dynamic influence of a valve and reducing throttle losses. The controller structure is designed from a model-based approach, where the electric motors and associated drives are operated in speed control modes. A sum and load pressure decoupling control structure is proposed, enabling the use of SISO control design for the pressure level and the load pressure separately. For the latter, a cascaded hydraulic drive controller structure is proposed, where the inner loop consists of a pressure controller, and the second and third loop consists of a velocity and position controller respectively. A method to smoothly switch from velocity to pressure control is furthermore proposed. Experimental results comparing injection cycles of an industrial injection moulding machine and the retrofitted injection drive and proposed control are presented.

Keywords: Electro-Hydraulic Variable-Speed Drive, Reference Switchover, Injection Moulding, Motion and Pressure Control

1. INTRODUCTION

The realizable bandwidth of a control system depends on the design of the system. Injection moulding machines are historically hydraulic driven, however in the last couple of decades electric machines are expanding in volume. The electric machines are marketed on performance related to speed, accuracy and energy consumption, which are important parameters in injection moulding [1]. An increase in speed can decrease cycle time, hence increasing the productivity. A desire of narrower tolerances in the produced part furthermore drives the demand for accuracy as it is expected that an increase in machine accuracy increases the part tolerances [2]. The primary benefit of hydraulic machines is the possibility of a higher power density and a cost-effective linear motion with hydraulic cylinders [3]. This is also seen as the purchasing cost of a hydraulic injection moulding machine is less compared to electrical machines according to [1]. The main focus of this paper is to examine the possibility of transferring the benefits of electric injection moulding machines to hydraulic moulding machines by employing electro-hydraulic variable-speed drives for the injection unit. While electro-hydraulic variable-speed drives are acknowledged for their energy efficiency [4], it is important to note that an in-depth investigation of energy efficiency lies beyond the scope of this study. The primary motivation behind this research is to assess if the benefits observed in electric moulding machines are transferable to hydraulic moulding machines using standard hydraulic components including feedback control of said components.

The type of hydraulic drive considered in this paper is classified within the field of electro-hydraulic variable-speed drives [5]. In this area various single cylinder drives with one or several pumps have been proposed and their properties considered in various ways [6–10], and also multi cylinder electro-hydraulic variable-speed drives are currently emerging [4, 11].

A hydraulic industrial state of the art injection moulding machine (SOA) is retrofitted with a dual pump drive (DPD), which essentially is a electro-hydraulic variable-speed drive shown in Fig. 1. This work focuses on a speed variable drive for an asymmetric cylinder. The design enables the possibility to increase the bandwidth compared to a valve controlled hydraulic injection moulding machine. In the design of the hydraulic system, the focus has been on removing throttle losses, which means that no valves are installed in the flow path between pumps and cylinder. The only valves in the flow path are check valves that

*Corresponding author: Rasmus.Aagaard.Hertz@LEGO.com

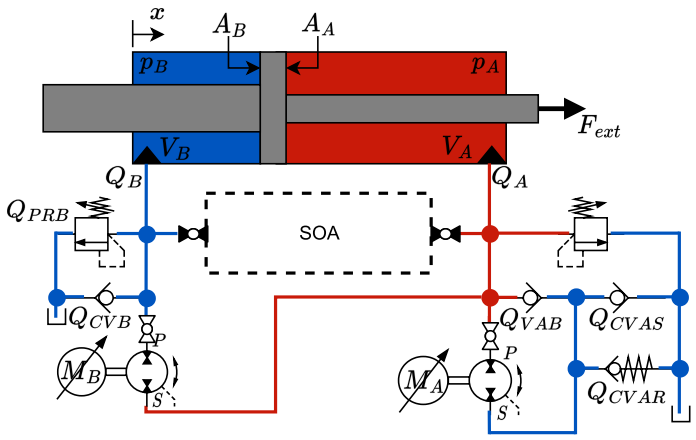

FIGURE 1: HYDRAULIC SCHEMATIC OF RETROFITTED SYSTEM.

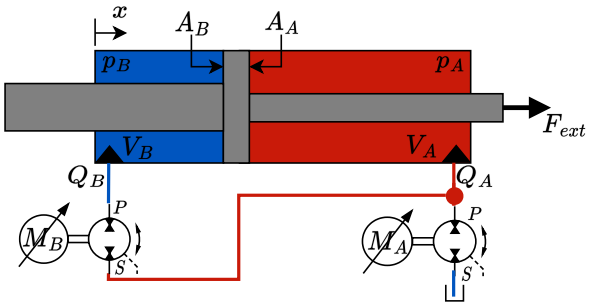

FIGURE 2: SIMPLIFIED HYDRAULIC SCHEMATIC OF RETROFITTED SYSTEM.

work as anti-cavitation safety. These valves operate with a small pressure drop, resulting in a small loss of efficiency. It is furthermore a focus to ensure individual control of both high- and low-pressure chambers of the injection cylinder, which is ensured using two motors and pumps. To minimise the size of pump B, the pump is connected between the high pressure and low pressure chamber, ensuring the pump only needs to account for the differential in volume between high and low pressure side. The sketch of the system can be seen in Fig. 1. A set of ball valves makes it possible to switch between the DPD and the SOA machine. The system can operate in four quadrant mode; however, both check valves and pressure relief valves will not be utilised in normal operation. The mentioned valves are $Q_{PRB}, Q_{CVBS}, Q_{PRA}, Q_{CVAR}, Q_{CVAP}$ and Q_{CVAS}. A simplified sketch of the system can be seen in Fig. 2.

The injection moulding process consists of multiple steps in order to push the molten plastic into the cavity inside the mould. With respect to the injection cylinder, the first step is to control the velocity of the ram, while filling the muold. When the mould is 99% full it is necessary to switch to pressure control in a smooth manner. The pressure control is kept at a constant reference until there is no flow into the mould. The machine should be capable of running with a wide range of moulds and materials that require robust controller design. Modeling and control of the system are based on physically motivated design principles following the methodology described in [4], as opposed to sophisticated algorithms like [12–14].

The system is a multi-input system due to the two controllable electric motors and a single output system being either the pressure, velocity, or position. It is desired to decouple the two motor inputs to allow SISO control of the load pressure and the sum pressure in the cylinder chamber. A cascaded control structure is proposed with an inner pressure controller and an outer motion controller. Lastly, a switchover method is described, switching from velocity to pressure control; however, the proposed structure enables the possibility to switch bidirectionally between two generic references smoothly.

2. SYSTEM MODEL

The system is modelled only considering the components used in normal operation, as seen in Fig. 2. The external force on the cylinder is dependent on material and mould, and will therefor vary. For the design of controllers the external force is seen as a disturbance. The pressure dynamics for chambers A and B are given by Eqs. (1) and (2).

$$\dot{p}_A = \frac{\beta_A}{V_A}(Q_A - Q_B - Q_{Lc} + A_A\dot{x}) \tag{1}$$

$$\dot{p}_B = \frac{\beta_B}{V_B}(Q_B + Q_{Lc} - A_B\dot{x}) \tag{2}$$

Where $A_A = 7.8 \cdot 10^{-3}$ m^2 and $A_B = 2.7 \cdot 10^{-3}$ m^2 is the effective area of the piston for each chamber. $Q_{Lc} = C_{Lc}(p_A - p_B)$, $C_{Lc} \cdot 10^{-16}$ m^3/Pa is the leakage across the cylinder piston from volume A to B. β_A and β_B is the bulk modulus of the oil. V_A and V_B is the volume of each chamber depending on the position x of the piston. $\dot{x}$ is the piston velocity. Q_A and Q_B are the pump flows. The bulk modulus of each chamber is given by Eq. 3.

$$\beta_n = \left(\frac{1}{\beta_{oil}} + \left(\frac{\epsilon_{air}}{n_{oil}p_n}\right)\right)^{-1} \tag{3}$$

Where $\beta_{oil} = 9.5 \cdot 10^9$ Pa is the maximum value of the bulk modulus of the oil. p_n is the chamber pressure, where $n = [A, B]$. $n_{oil} = 1.4$ is the polytropic exponent and ϵ_{air} is given by Eq.

$$\epsilon_{air} = \epsilon_{air,0}\left(\frac{p_{atm}}{p_n}\right) \tag{4}$$

Where $\epsilon_{air,0} = 0.005$ % is the percentage of air in the oil at atmospheric pressure and $p_{atm} = 10^5$ Pa is the atmospheric pressure. The Volumes V_A and V_B are calculated by Eq. (5)

$$V_A = V_{A,I} + A_A(L - x), \qquad V_B = V_{B,I} + A_B x \tag{5}$$

Where $V_{A,I} = 1.4 \cdot 10^{-3}$ m^3 and $V_{B,I} = 1.6 \cdot 10^{-3}$ m^3. The pump flows Q_A and Q_B are given by Eq. (6)

$$Q_A = D_A\omega_{mA} - k_A Q_{LPA}, \qquad Q_B = D_B\omega_{mB} - k_B Q_{LPB} \tag{6}$$

Where the pump dicplacemts $D_A = 16$ ccm/rev and $D_B = 8.1$ ccm/rev. ω_{mA} and ω_{mB} is the angular velocity. $Q_{LPA} = Q_{LPA}(p_B, p_A, \omega_A)$ and $Q_{LPB} = Q_{LPB}(p_B, p_A, \omega_B)$ are the internal leakage in the pump estimated from [15] and scaled according to displacement fraction. The scaling is $k_A = 0.592$ and $k_B = 0.296$. The piston velocity dynamics are given in Eq. (7)

$$\ddot{x} = \frac{1}{m}(-p_A A_A + p_B A_B - F_C sgn(\dot{x}) - B_v\dot{x} + F_{ext}) \tag{7}$$

Where $m = 250$ kg is the mass of the injection unit, $B_v = 6480 \frac{\text{N·s}}{\text{m}}$ is the viscous friction, $F_C = 1241$ N is the columb friction and sgn is the sigmoid function to make the function continues.

The motor dynamics are modelled as a second order system. Parameters are estimated through the drive software, performing a range of step inputs to the velocity reference on the drive. The parameters are estimated to a damping of 0.7 and a natural frequency of 127 Hz.

3. STATE DECOUPLING

As an injection moulding machine runs with multiple moulds and materials it is desired to utilise well known and robust controllers that are well understood. Linear SISO controllers are both well understood and intuitive with respect to tuning and error handling. To enable SISO control of a multi-input single output system couplings between actuators needs to be considered.

3.1 Input Output Coupling Analysis

The interaction of the inputs to the system with the output of the system can be analyzed using the relative gain array (RGA) analysis for linear systems. As the system equations are nonlinear, it is necessary to linearize those before it is possible to perform the analysis. The leakage across the pumps and piston is neglected. It is further assumed that the motor velocity loop is sufficiently fast to neglect the motor dynamics. The linearization is based on Taylor expansion at an equilibrium point. The state vector is defined as $\mathbf{x} = \begin{bmatrix} x & \dot{x} & p_A & p_B \end{bmatrix}^T$. The Taylor expansion for the chamber pressure gradients are given in eq. Eqs. (8) - (9).

$$\begin{aligned}\Delta \dot{p}_{AL} =& \frac{\partial \dot{p}_A}{\partial x}\bigg|_{\mathbf{x}_0} \Delta x + \frac{\partial \dot{p}_A}{\partial \dot{x}}\bigg|_{\mathbf{x}_0} \Delta \dot{x} + \frac{\partial \dot{p}_A}{\partial p_A}\bigg|_{\mathbf{x}_0} \Delta p_A + \frac{\partial \dot{p}_A}{\partial p_B}\bigg|_{\mathbf{x}_0} \Delta p_B + \\ & \frac{\partial \dot{p}_A}{\partial \omega_A}\bigg|_{\mathbf{x}_0} \Delta \omega_A + \frac{\partial \dot{p}_A}{\partial \omega_B}\bigg|_{\mathbf{x}_0} \Delta \omega_B \end{aligned} \tag{8}$$

$$\begin{aligned}\Delta \dot{p}_{BL} =& \frac{\partial \dot{p}_B}{\partial x}\bigg|_{\mathbf{x}_0} \Delta x + \frac{\partial \dot{p}_B}{\partial \dot{x}}\bigg|_{\mathbf{x}_0} \Delta \dot{x} + \frac{\partial \dot{p}_B}{\partial p_A}\bigg|_{\mathbf{x}_0} \Delta p_A + \frac{\partial \dot{p}_B}{\partial p_B}\bigg|_{\mathbf{x}_0} \Delta p_B + \\ & \frac{\partial \dot{p}_B}{\partial \omega_A}\bigg|_{\mathbf{x}_0} \Delta \omega_A + \frac{\partial \dot{p}_B}{\partial \omega_B}\bigg|_{\mathbf{x}_0} \Delta \omega_B \end{aligned} \tag{9}$$

Where $\mathbf{x}_0 = [x_0\ \dot{x}_0\ p_{A0}\ p_{BO}\ \omega_{A0}\ \omega_{B0}]^T$ is the equilibrium point. The cylinder position will vary, to determine x_0 a pole sweep, and the position with the lowest damping for the 4 combinations of in and output is used for the coupling analysis corresponding to $x_0 = L$. The controller is designed to maintain a minimum pressure in the low-pressure chamber, which is $p_{BO} = p_{set}$. From this it is possible to calculate the equilibrium point from $\dot{p}_A = 0$ and $\dot{p}_B = 0$ as Eq. (10).

$$\begin{aligned} x_0 =& L \\ \dot{x}_0 =& 0 \\ p_{A0} =& \frac{F_{ext} + p_{B0} A_B}{A_A} \\ p_{BO} =& p_{set} \\ \omega_{A0} =& -\frac{D_B \omega_{B0}}{D_A} \\ \omega_{B0} =& 0 \end{aligned} \tag{10}$$

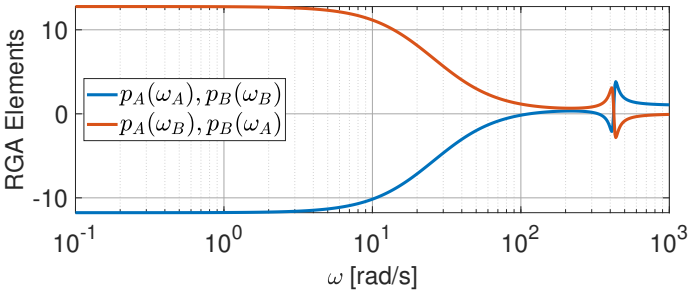

FIGURE 3: RGA ELEMENTS OF THE ORIGINAL SYSTEM. CHANGING BEST PAIRINGS ARE PRESENT ACROSS THE FREQUENCY RANGE BETWEEN MOTOR INPUTS AND CHAMBER PRESSURES.

Where $F_{ext} = 27000$ N and $p_{set} = 30 \cdot 10^5$ Pa. The linearised chamber volumes are given in Eqs. (11) - (12).

$$V_{A,0} = V_{A,I} + A_A(L - x_0) \tag{11}$$

$$V_{B,0} = V_{B,I} + A_B x_0 \tag{12}$$

The state space representation of the linear system is derived based on Eqs. (7)-(12) and given in Eq. (13).

$$\dot{\mathbf{x}} = \mathbf{A}\mathbf{x} + \mathbf{B}\mathbf{u}, \quad \mathbf{y} = \mathbf{C}\mathbf{x}, \quad \mathbf{x} = \begin{bmatrix} x & \dot{x} & p_A & p_B \end{bmatrix}^T \tag{13}$$

$$\mathbf{u} = \begin{bmatrix} \omega_A & \omega_B \end{bmatrix}^T, \quad \mathbf{A} = \begin{bmatrix} 0 & 1 & 0 & 0 \\ 0 & -\frac{B_v}{m} & -\frac{A_A}{m} & \frac{A_B}{m} \\ 0 & \frac{\beta_0}{V_{A,0}} A_A & 0 & 0 \\ 0 & -\frac{\beta_0}{V_{b,0}} A_B & 0 & 0 \end{bmatrix}$$

$$\mathbf{B} \begin{bmatrix} 0 & 0 \\ 0 & 0 \\ \frac{\beta_0}{V_{A,0}} D_A & -\frac{\beta_0}{V_{A,0}} D_B \\ 0 & \frac{\beta_0}{V_{B,0}} D_B \end{bmatrix}, \quad \mathbf{C} \begin{bmatrix} 0 & 0 & 1 & 0 \\ 0 & 0 & 0 & 1 \end{bmatrix}$$

Based on the lineariezed coefficients $\beta_0 = 9.5 \cdot 10^8$ Pa, $V_{A,0} = 1.4 \cdot 10^{-3}$ m^3 and $V_{B,0} = 2.0 \cdot 10^{-3}$ m^3 it is possible to calculate the transfer function matrix between the input motor velocities ω_A and ω_B and the chamber pressure p_A and p_B from Eq. (14).

$$\mathbf{G} = \mathbf{C}(s\mathbf{I} - \mathbf{A})^{-1}\mathbf{B} \tag{14}$$

The RGA elements are plotted in Fig. 3, showing significant couplings between both motor velocities and the chamber pressures as expected from the design as e.g. motor B is connected between the two cylinder chambers. The proposed decoupling strategy is based on an input and output decoupling, on the nonlinear time domain model. This takes into account the volume and pressure variations in the system. The leakage flows are neglected in the decoupling and considered a disturbance as the leakage flows are much smaller than the pump flows.

3.2 Output Decoupling

The output decoupling is created based on two virtual pressures related to force (p_L) and pressure level (p_H) given in Eq. (15) .

$$p_L = p_A - \alpha p_B, \quad p_H = p_A + p_B \tag{15}$$

Where $\alpha = \frac{A_B}{A_A}$.

4. INPUT DECOUPLING

The input decoupling seeks to calculate the desired speed of the two motors to control the pressure and motion of the cylinder. This can be achieved by multiple methods. The input decoupling strategy is based on a desire for the closed loop pressure dynamics to behave as first order systems given in Eq. (16).

$$\dot{p_L} = \omega_L(p_L^* - p_L), \quad \dot{p_H} = \omega_H(p_H^* - p_H) \tag{16}$$

Where "$\bullet^*$" is the reference. ω_L and ω_H is related to the time constants as $\omega_n = \frac{1}{\tau_n}$ of the desired first order dynamics, and should be chosen in the range of 5-10 times below the natural frequency of the motors eigenfrequency.

The differentiation of the output decoupling given in Eq. (15) with respect to time is shown in Eq. (17).

$$\dot{p_L} = \dot{p_A} - \alpha \dot{p_B}, \quad \dot{p_\Sigma} = \dot{p_A} + \dot{p_B} \tag{17}$$

Using Eqs. (1), (2), (16) and (17) the pressure dynamics can be rewritten and it is possible to solve for the two pump flows Q_A and Q_B. If p_L^* and p_H^* are known and it is possible to measure p_L, p_H and x, the only unknown variables are β_A, β_B and $\dot{x}$. Common for these are that they are either not possible to measure directly or prone to noise due to numerical differentiation, however if the estimated values denoted by "$\tilde{\bullet}$" are used the pump flows can be calculated as given in Eqs. (18) - (21). It is furthermore assumed that $\beta_A = \beta_B$ due to the desire of a minimum pressure in the low-pressure chamber.

$$\omega_A = \psi_1(-p_L^* + p_L) + \psi_2(p_H^* - p_H) - \frac{(A_A - A_B)}{D_A}\tilde{\dot{x}} \tag{18}$$

$$\omega_B = \psi_3(p_L^* - p_L) + \psi_3(p_H^* - p_H) + \frac{A_B}{D_B}\tilde{\dot{x}} \tag{19}$$

Where

$$\psi_1 = \frac{\omega_L(V_A \cdot -V_B)A_A}{\tilde{\beta}(A_A + A_B)D_A}, \quad \psi_2 = \frac{\omega_H(A_A V_B + A_B V_A)}{\tilde{\beta}(A_A + A_B)} \tag{20}$$

$$\psi_3 = \frac{V_B A_A}{\tilde{\beta}(A_A + A_B) * D_B} \tag{21}$$

It is now possible to calculate the desired pump flows depending on the load pressure and sum pressure references if the given parameters are measured and estimated. The measurements should be low noise and high bandwidth to ensure minimum influence on the dynamic system. The drawback of the mentioned method is that the estimated velocity and bulk modulus needs to be known. The estimation of velocity can be a significant drawback when running the system in pressure control at speeds different from approximately zero. A solution could be to estimate the speed with e.g. a Kalman filter or sliding-mode observer. A steady state error can be present as there is no integrator effect if the parameters of the system is estimated with errors, or the leakage of the system is large. If it is possible to estimate e.g. the leakage it could be taken into account when designing the input decoupling.

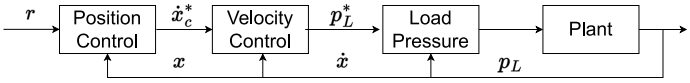

FIGURE 4: CASCADED CONTROLLER STRUCTURE

5. SUM PRESSURE REFERENCE

From the decoupled system it is possible to control the load pressure and sum pressure. The load pressure is linearly dependent on the cylinder force, and the reference will be based on either a required force or generated from a motion controller. The reference for the sum pressure is, however, not as intuitive. It will be used to control the low pressure side of the cylinder ensuring a minimum pressure in the system. This is desired to keep the bulk modulus at a high level, ensuring a stiff system. The sum pressure reference is constructed to ensure a minimum pressure p_{set} in the low pressure side of the cylinder. To ensure high stiffness in the oil and cylinder, the minimum pressure is chosen to be $p_{set} \geq 30$ bar. The sum pressure reference P_H^* is chosen depending on the pressures in chamber p_A and p_B according to Eqs: (22) and (23)

$$\text{if} \quad p_A \geq p_B, \quad P_H^* = p_A + p_{set} \tag{22}$$

$$\text{if} \quad p_A < p_B, \quad P_H^* = p_{set} + p_B \tag{23}$$

This ensures a pressure of p_{set} in the low-pressure chamber without any discontinuities in the reference to the controller. This is in principle a feedback loop that should be taken into account when accessing stability of the system.

6. MOTION CONTROL

As the velocity trajectory is utilised in the input decoupling it is important to ensure the trajectory is continues and differentiable to avoid jumps in the angular motor velocity reference. To ensure a seamless trajectory, the objective is to achieve a smooth and differentiable path that begins with a zero initial condition for position and its derivatives up to the sixth derivative, commonly referred to as the piston's "crackle" [16, 17]. . It is also important to have a well-designed motion controller to ensure tracking of the desired trajectory.

The motion controller will be based on a position and velocity controller. The controller will be designed based on a cascaded controller structure shown in Fig. 4. The benefit of the cascaded control structure is that it is possible to set the inner loops to a unit gain, which means $p_L^* = p_L$. However to enable that assumption each outer loop needs to be designed so it is 5-10 times slower than the previous loop. For this setup, the bandwidth of the load pressure, velocity, and position will be 25, 5 and 1 Hz, respectively.

6.1 Velocity Controller

Due to the cascaded control structure, it is possible to design the motion controller based on Eq. (7), however before it is

desired to rewrite it in terms of the the load pressure p_L given in 15. The equation is linearized assuming that the external force (F_{ext}) and the static friction (F_C) are disturbances to Eq. (24).

$$\ddot{x} = \frac{1}{m}(A_A p_L - B_v \dot{x}) \tag{24}$$

From the linear expression, the transfer function $\frac{\dot{x}}{p_L^*}$ shown in Eq. (25) can be constructed.

$$\frac{\dot{x}}{p_L^*} = \frac{A_A}{ms + B_v} \tag{25}$$

A PI controller is utilised, the control law is stated in Eq. (26).

$$p_L^* = K_{Pv}(\dot{x}^* - \dot{x}) + \frac{K_{Iv}}{s}(\dot{x}^* - \dot{x}) \tag{26}$$

The controller constants are designed to achieve a bandwidth of 5 Hz. This may be achieved considering a first order system with cut of frequency at 5 Hz, see Eq. (27).

$$\frac{\dot{x}}{\dot{x}^*} = \frac{\omega_{cv}}{s + \omega_{cv}} \tag{27}$$

Where ω_{cv} is the cut-off frequency. Using Eq. (25)-(27) it is possible to calculate the velocity controller gains to:

$$K_{Pv} = \frac{m\omega_{cv}}{A_A}, \quad K_{Iv} = \frac{B_v \omega_{cv}}{A_A} \tag{28}$$

Effectively, the controller will cancel out the system pole and ensure the bandwidth is at the desired 5 Hz.

6.2 Position Control

The position contoller is a simple proportional controller due to the inherent integrator effect when transferring from position to velocity. The control law can be stated as Eq. (29).

$$\dot{x}^* = \dot{r} + K_{Pp}(x^* - x) \tag{29}$$

K_{Pp} is found using a similar approach to determining the controller gains of the velocity PI controller to:

$$K_{Pp} = \omega_{cp} \tag{30}$$

ω_{cp} is the cut of frequency of the position controller determined to 1 Hz.

7. SWITCHOVER

Ensuring a smooth load pressure reference for the full moulding process, is important when enabling the switchover between the velocity controlled fill phase and the pressure controlled holding phase, as it where the plastic is packed to create elements with stable parts [18]. The switchover between two controllers have some inherent challenges as continues states is needed for this to be smooth. The bumpless transfer problem is defined by [19] as the transfer or switch between one closed loop controller to another acting on a plant. In general two approaches are taken; one approach is to let the second controller track the first controller, and the second approach is to match the states between the controllers [19–25] etc.

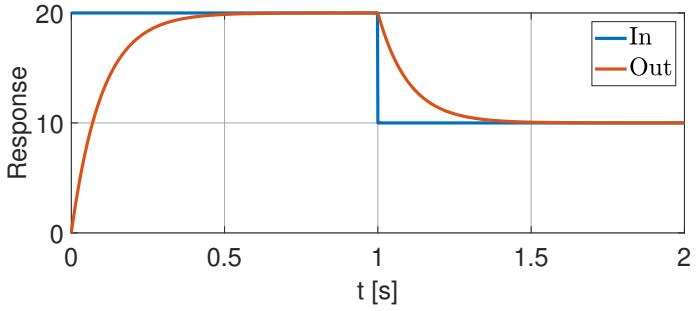

FIGURE 5: CONTIUES TIME RESPONSE OF A STEP INPUT TO A LPF.

The method proposed in this work takes advantage of the cascaded controller structure shown in Fig. 4. The problem is as such reduced to creating a continuous reference to the inner pressure loop controller independent of the finishing point of the motion controller pressure reference and the starting point of the pressure controller reference[18]. As any oscillations in the transition is undesired, the ideal transition would be similar to a first order response more specifically as a low pass filter (LPF). If it is possible to design a reference following a first order response it is furthermore possible to control the settling time before the new set reference is achieved. First consider a LPF in continues time shown in Eq. (31).

$$\frac{P_L^*}{e} = \frac{\omega_f}{s + \omega_f} \tag{31}$$

Where ω_f is the filter cut of frequency. This filter will ensure a continuous output if it is provided a step input similar to the switch between the two references. The settling time is directly correlated to the filter frequency ω_f through $t_{set} = \frac{4}{\omega_f}$. Figure 5 shows the response of the step change in reference to the proposed LPF with a first step at $t = 0$ s to a value of 20 and a second step at $t = 1$ s to a value of 10. The filter frequency $\omega_f = 10$ rad/s. As expected, the output of the filter is smooth and continues, with a settling time of approximately 0.4 s. The drawback, however, is that the filter adds a phase delay to both desired references when considered in the continues time domain. As it is necessary to dicretise the LPF for implementation on a e.g. plc, lets consider the discretised form of the LPF as described in Eq. (32).

$$p_{L,r}^*(k) = \frac{e(k)\omega_f T_s + e(k-1)\omega_f T_s - p_L^*(k-1)(\omega_f T_s - 2)}{2 + \omega_f T_s} \tag{32}$$

Where T_s is the sampling frequency, $e(k)$ and $e(k-1)$ is the current input and previous input to the filter. $p_{L,r}^*(k)$ and $P_L^*(k-1)$ is the current and previous input to the load presssure controller.

In the discrete version of the filter, it is possible to locate the previous input $P_L^*(k-1)$ to the load pressure controller, as a parameter which was not possible in the continues case showcased in Eq. (31) and Fig. 5 where the parameter was hidden.

This enables the possibility of using two filters as shown in Fig. 6. It is a simple and robust method to do switchover between two references to a controller, however if a dynamic reference is

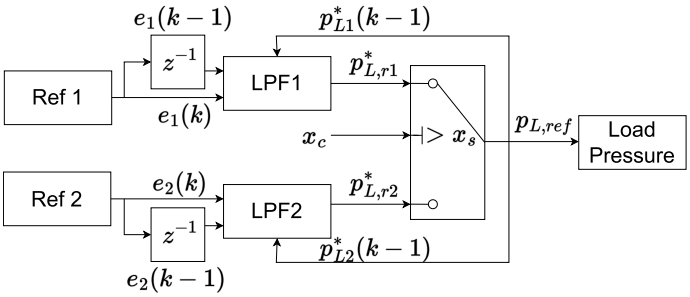

FIGURE 6: BLOCK DIAGRAM FOR SWITCHOVER APPROACH BETWEEN TWO CONTROLLERS WITH LOW PASS FILTER.

desired it will as discussed introduce a phase delay dependent on the filter frequency. In the given application, it is not necessary to switch back to the first reference again, meaning that only LPF2 is utilized, ensuring no phase delay on the motion controller reference to the load pressure controller. The switchover criteria can be chosen independently, in injection moulding multiple possible switchover criteria are proposed. In the work presented here, the position is chosen as the switchover criterion.

8. EXPERIMENTAL RESULTS

The dual pump drive is retrofitted on the SOA. The retrofit is constructed from the schematic in Fig. 1. The motors are permanent magnet synchronous motors and the pumps are axial piston pumps with 9 cylinders each. The controller communicates with the drives and the analog to digital converters over etherCAT® with a clock frequency of 2 ms. The pressure controller is first tested independently, following a no load position and velocity controller test. Having tested the pressure and velocity controller, a full load cycle is tested including switchover. This test includes the unknown load from plastic and mould. Lastly, a comparison to the SOA and DPD is performed.

8.1 Pressure Control

The pressure control is tested, by moving the cylinder to $x = 0$ mm. A load pressure trajectory is designed that randomly includes multiple steps in pressure; see Fig. 7a. The test is created based on step input, as it is seen as the most difficult to handle as it excites all frequencies in the system. In normal operation, the machine will not be given step input to either pressure, velocity, or position controller as described previously. Simulation and experimental data from the DPD are given in Fig. 7b. The controller parameters are $\omega_L = 80$ rad/s, $\omega_H = 60$ rad/s, $\tilde{x} = 0$ m/s, $p_{set} = 30 \cdot 10^5$ Pa and $\tilde{\beta}_A = \tilde{\beta}_B = 9.5 \cdot 10^8$ Pa. Theoretically, it is possible to design the controller values of ω_L and ω_H in the range of 160 rad/s, however, due to noise and sample delay in the physical setup, this is not feasible. In a high gain loop noise will be amplified rendering the system unstable. The sample delay of the controller adds additional unmodelled phase to the system, and if this phase shift becomes too large, the controller becomes unstable. There is good agreement between experimental and simulated data. A small steady state error can be seen due to the leakage of the pump and cylinder, as the leakage terms are not included in the controller design. It is further seen that the experimental data have an overshoot depending on the step size.

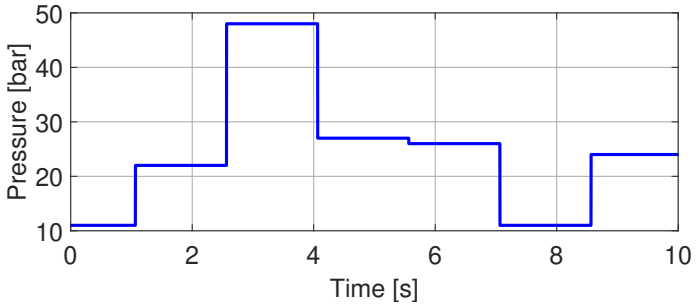

(a) Reference to the load pressure controller p^*_L.

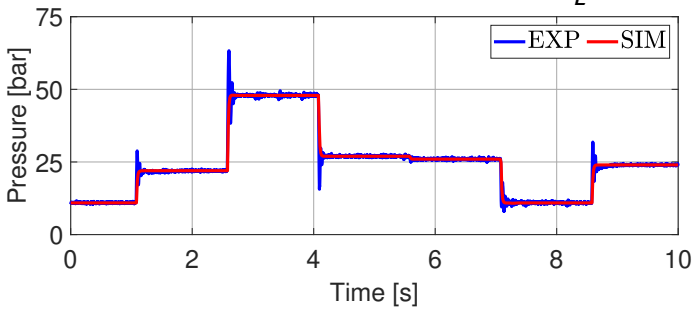

(b) Load pressure p_L

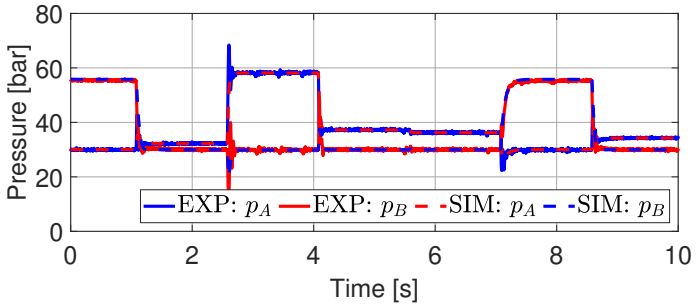

(c) Chamber pressure p_A and p_B.

FIGURE 7: LOAD PRESSURE CONTROLLER PERFORMANCE.

The overshoot can be caused by multiple things such as model inaccuracies etc., however it is not a problem in situations where the pressure is ramped. From Fig. 7c it is observed that the low-pressure side is always kept at approximately $p_{set} = 30 \cdot 10^5$ Pa.

8.2 Velocity Control

Due to the design of the injection moulding machine, it is not possible to test the position and velocity controller with a known force, for that reason a no load velocity control test has been performed. The cylinder has been placed away from the ends to ensure that no end effects are present in the experiment. A trajectory is generated as shown in Fig. 8a. The pressure controller values are, $\omega_L = 100$ rad/s, $\omega_H = 80$ rad/s, $\tilde{x} = \dot{x}^*_c + \dot{r}$ m/s and $\tilde{\beta}_A = \tilde{\beta}_B = 9.5 \cdot 10^8$ Pa. The position and velocity controller values are, equal to Eq. (28) and (30) with $\omega_{cp} = 2 * \pi$ rad/s.

The simulation and experimental results are shown in Fig. 8. It is the velocity that is of interest in injection moulding, for that reason the plot of the cylinder position is omitted. The position error is less than 2 mm at all times on the experimental setup.

Instead, the velocity is an important process parameter. The experimental and simulated results can be seen in Fig. 8. From Fig. 8b it is seen that the velocity tracking is good, however, the physical system does have a delay compared to the simulation. Considering the error shown in Fig. 8c, it is seen that in the main part of the trajectory it is less than 1 mm/s for the no load test. The error is larger in the beginning which possibly could be reduced by minimizing the jerk limit of the trajectory. Only a slight change in the chamber pressure is seen in Fig. 8d as there is no load on the cylinder. The minimum chamber pressures are equal to p_{set}. Generally, it can be seen that the controller has good tracking performance and there is a good agreement between simulation and experimental results.

8.3 Full Process

The load pressure, level pressure, and motion controller, including the switchcover capability between the motion and load pressure controller, is tested through injection moulding tests. The load from the molten plastic that is forced into the closed mould is unknown. The injection moulding trajectory starts around 30 mm, the cylinder should be velocity controlled until 11 mm, corresponding to the distance it takes to fill the mould. After filling the mould, the cavities should be after packed utilising pressure control. This means that the velocity controller needs to switch to the pressure controller with a constant pressure reference.

The controller have been tuned due to the dynamics of the loading, it is expected to mainly be from a viscous component of the external force. The pressure controller values are, $\omega_L = 100$ rad/s, $\omega_H = 80$ rad/s, $\tilde{\dot{x}} = \dot{x}_c^* + \dot{r}$ and $\tilde{\beta}_A = \tilde{\beta}_B = 9.5 \cdot 10^8$ Pa. The trajectory is based on velocity of 38 mm/s. The motion controller gains are $K_{Iv} = 38.88 \cdot 10^7 \frac{\text{Pa}\cdot s}{\text{m}}$, $K_{Pv} = 1.5 \cdot 10^7 \frac{\text{Pa}\cdot s}{\text{m}}$ and $K_{Pp} = 16\ \text{s}^{-1}$. The switchover filter frequency for both p_L and $\tilde{\dot{x}}$ are 12 rad/s.

From Fig. 9 the response of the full moulding process is shown. First note the switchover occuring at approximately 0.75 s. Up to this point, the process is controlled by the motion controller as recognized in Fig. 9a. The velocity controller reference stops when the switchover occurs, however, the reference to the load pressure controller is continues as seen in Fig. 9a-9c. The velocity controller tracks the reference well on the ramped section, but has an error when the velocity is supposed to be constant. This is most likely due to external forces that can change almost instantly due to the mould geometry. After the switchover it is seen that the pressure follows the reference with almost zero steady state error. It is possible to change the switchover time dependent on the filter frequency. In injection moulding, it is important that the load pressure reference is achieved without an undershoot, which can occur if the switchover happens at a larger bandwidth than the controller is capable of. It is seen from Fig. 9b that the reference to the load pressure controller p_L^* is smooth and continues.

8.4 Comparison between DPD and SOA

To compare the SOA and DPD the mould is run with the same settings on both sets of equipment. The controller parameters are the same as in Section 8.3. The target velocity before switchover is

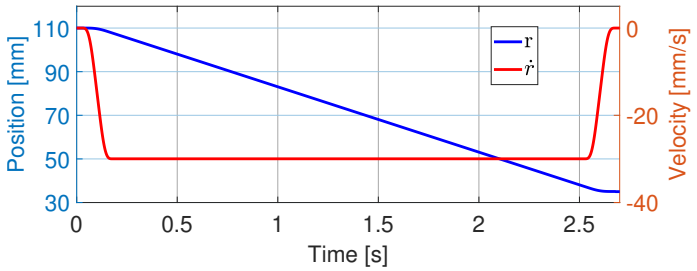

(a) Motion controller trajectory

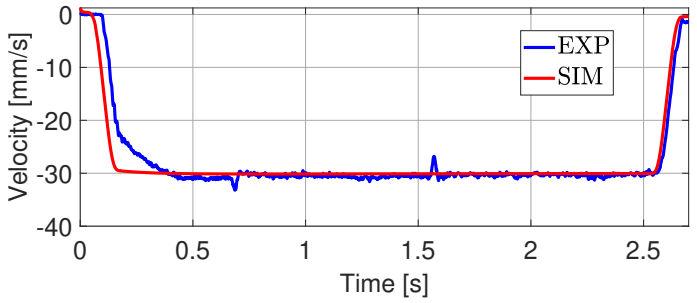

(b) Cylinder velocity $\dot{x}$.

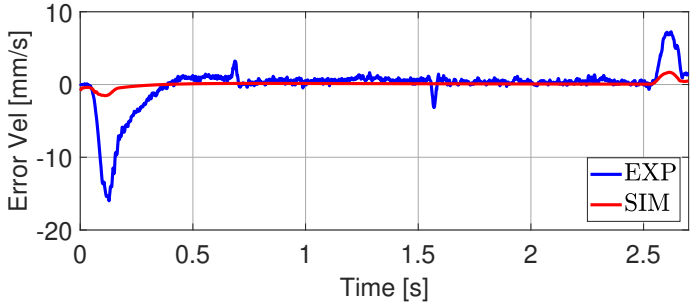

(c) Cylinder velocity error.

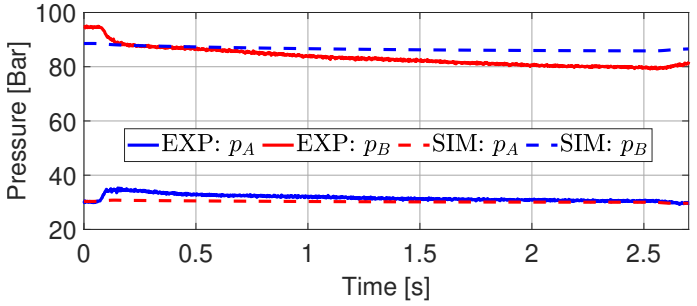

(d) Chamber pressures.

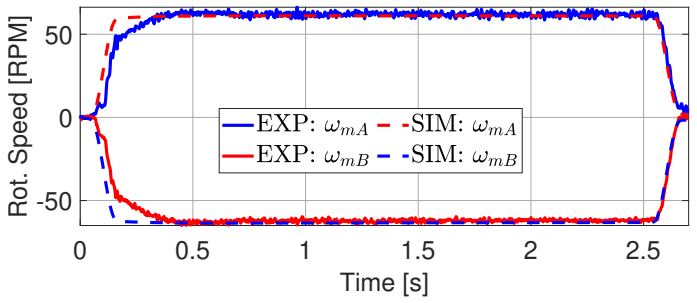

(e) Motor angular velocity.

FIGURE 8: MOTION CONTROLLER PERFORMANCE, EVALUATED ON THE DPD AND SIMULATION.

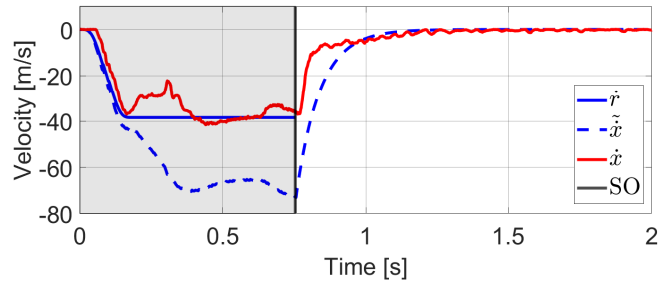

(a) Trajectory

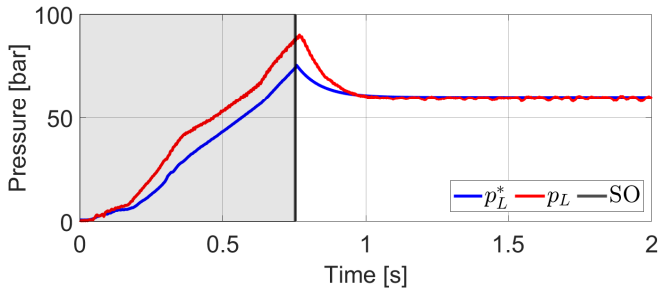

(b) Load pressure (p_L).

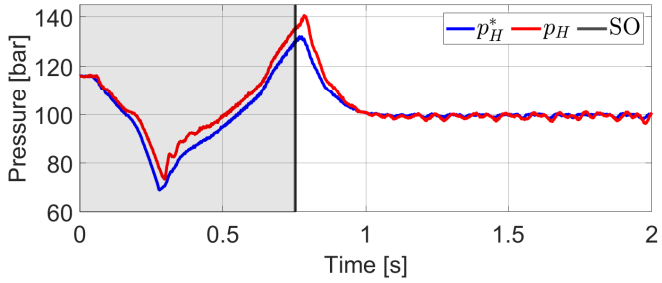

(c) Sum pressure (p_H).

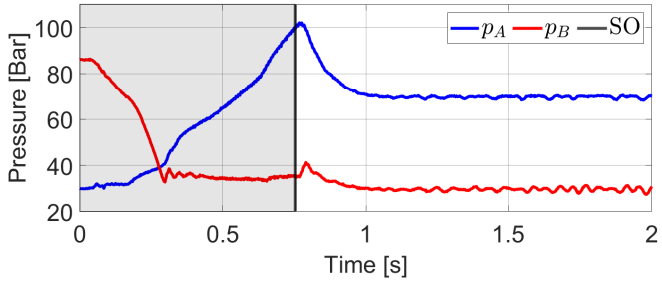

(d) Chamber pressures.

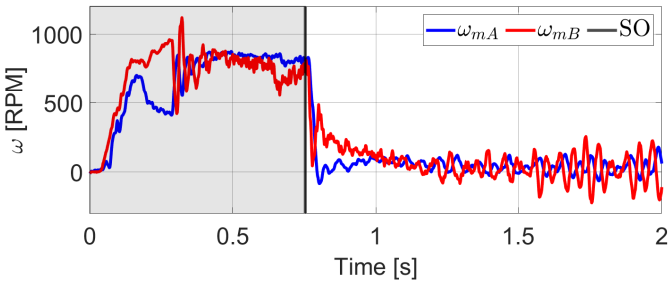

(e) Motor angular velocity.

FIGURE 9: POSITION AND VELOCITY CONTROLLER INCL. SWITCHOVER (SO) FOR THE FULL MOULDING CYCLE.

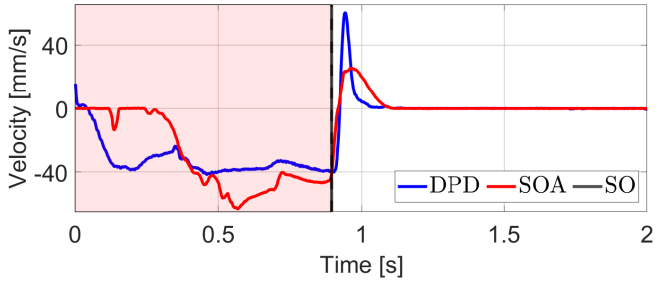

(a) Velocity.

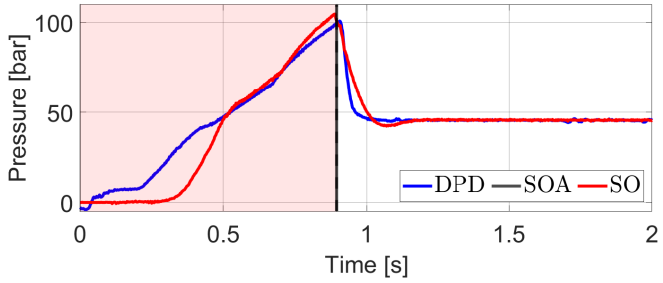

(b) Trajectory

FIGURE 10: PERFORMANCE COMPARISON BETWEEN DPD AND SOA.

$\dot{r} = 40$ mm/s, and the load pressure reference after the switchover is $p_L^* = 45.5 \cdot 10^5$ Pa. The switchover filter cut off frequency is $\omega_f = 80$ rad/s. The moulding process is adjusted to increase the difficulty of the switchover by switchover later than desired meaning the mould approaches 100% full to a lower holding pressure. This can occur in running production due to change in the raw material. The load pressure and velocity is seen in Fig. 10. It can be seen in Fig. 10a that the DPD setup is closer to the desired velocity in the period before the switchover. It is also approaching the holding pressure reference without any undershoot and at a faster rate than the SOA. The controllers and controller structure of the industrial machine is unknown. Overall it can be stated that the retrofitted system however shows improved tracking performance both within velocity control, switchover and pressure control.

9. CONCLUSION

A retrofit for a hydraulic state of the art injection moulding machine is designed, enabling motion and load pressure control. The controller is derived based on a physically motivated model of the hydraulic system. This enables the control of the pressure in each chamber, making it possible to ensure a minimum stiffness of the system through the sum pressure controller. Through decoupling it has been possible to control both the sum pressure and load pressure with SISO controllers. A motion controller is designed based on a simple proportional and PI controller. A smooth trajectory is designed ensuring no sudden jumps occurring in position, velocity, acceleration, jerk, snap or crackle. The initial condition for all time derivatives are furthermore zero. All controllers are implemented on the machine and successfully tested individually. The load pressure controller tracks the ref-

erence well, even for step inputs up to 30 bar. It furthermore keeps the low pressure side at the desired pressure level of 30 bar. Good agreement between simulation and experiment is seen. The motion controller is first tested in a no load situation, as it is not enabled to load the injection moulding machine with a well known force. The simulation and experiment both show good tracking performance as expected from the design. In the starting ramp an error of approximately 10 mm/s is seen, however it is fast decreasing to less than 1 mm/s. The error in the beginning could probably be minimised by slowing down jerk in the trajectory. Lastly a test with an injection moulding cycle is shown, where motion control, switchover and load pressure control is achieved successfully. In comparison with the SOA machine improvements is seen in all three phases of the process, namely within velocity control, switchover and pressure control.

ACKNOWLEDGMENTS

This work is funded by LEGO System A/S.

REFERENCES

[1] Kelly, A.l., Woodhead, M. and Coates, P.d. "Comparison of Injection Molding Machine Performance." *Polymer Engineering & Science* Vol. 45 No. 6 (2005): pp. 857–865. DOI 10.1002/pen.20335.

[2] Hertz, Rasmus Aa, Christensen, J. K., Kristiansen, S., Therkelsen, O. and Schmidt, L. "In-Line Process and Material Property Measurement in Injection Moulding - a Theoretical Review." *Production & Manufacturing Research* Vol. 10 No. 1 (2022): pp. 938–963. DOI 10.1080/21693277.2022.2148136.

[3] Helduser, Siegfried. "Electric-Hydrostatic Drive Systems and Their Application in Injection Moulding Machines." *Proceedings of the JFPS International Symposium on Fluid Power* Vol. 1999 No. 4 (1999): pp. 261–266. DOI 10.5739/isfp.1999.261.

[4] Schmidt, Lasse and Hansen, Kenneth Vorbøl. "Electro-Hydraulic Variable-Speed Drive Networks—Idea, Perspectives, and Energy Saving Potentials." *Energies* Vol. 15 No. 3 (2022): p. 1228. DOI 10.3390/en15031228.

[5] Ketelsen, Søren, Padovani, Damiano, Andersen, Torben O., Ebbesen, Morten Kjeld and Schmidt, Lasse. "Classification and Review of Pump-Controlled Differential Cylinder Drives." *Energies* Vol. 12 No. 7 (2019): p. 1293. DOI 10.3390/en12071293.

[6] Ketelsen, Søren, Andersen, Torben Ole, Ebbesen, Morten Kjeld and Schmidt, Lasse. "Mass Estimation of Self-Contained Linear Electro-Hydraulic Actuators and Evaluation of the Influence on Payload Capacity of a Knuckle Boom Crane." *ASME/BATH 2019 Symposium on Fluid Power and Motion Control*. 2019. American Society of Mechanical Engineers Digital Collection. DOI 10.1115/FPMC2019-1689.

[7] Padovani, Damiano, Ketelsen, Søren and Schmidt, Lasse. "Downsizing the Electric Motors of Energy-Efficient Self-Contained Electro-Hydraulic Systems by Using Hybrid Technologies." *BATH/ASME 2020 Symposium on Fluid Power and Motion Control*. 2020. American Society of Mechanical Engineers Digital Collection. DOI 10.1115/FPMC2020-2717.

[8] Ketelsen, Søren, Michel, Sebastian, Andersen, Torben O., Ebbesen, Morten Kjeld, Weber, Jürgen and Schmidt, Lasse. "Thermo-Hydraulic Modelling and Experimental Validation of an Electro-Hydraulic Compact Drive." *Energies* Vol. 14 No. 9 (2021): p. 2375. DOI 10.3390/en14092375.

[9] Schmidt, Lasse, Ketelsen, Søren, Grønkær, Nikolaj and Hansen, Kenneth Vorbøl. "On Secondary Control Principles in Pump Controlled Electro-Hydraulic Linear Actuators." *BATH/ASME 2020 Symposium on Fluid Power and Motion Control*. 2020. American Society of Mechanical Engineers Digital Collection. DOI 10.1115/FPMC2020-2722.

[10] Ketelsen, Søren, Andersen, Torben Ole, Ebbesen, Morten K. and Schmidt, Lasse. "A Self-Contained Cylinder Drive with Indirectly Controlled Hydraulic Lock." Vol. 41 No. 3 (2020): pp. 185–205. DOI 10.4173/mic.2020.3.4.

[11] Schmidt, Lasse, Ketelsen, Søren and Hansen, Kenneth Vorbøl. "Perspectives on Component Downsizing in Electro-Hydraulic Variable-Speed Drive Networks." *BATH/ASME 2022 Symposium on Fluid Power and Motion Control*. 2022. American Society of Mechanical Engineers Digital Collection. DOI 10.1115/FPMC2022-89547.

[12] Schmidt, Lasse and Andersen, Torben O. "Application of Second Order Sliding Mode Algorithms for Output Feedback Control in Hydraulic Cylinder Drives with Profound Valve Dynamics." *e & i Elektrotechnik und Informationstechnik* Vol. 133 No. 6 (2016): pp. 238–247. DOI 10.1007/s00502-016-0425-7.

[13] Schmidt, Lasse, Andersen, Torben O. and Pedersen, Henrik C. "On Application of Second Order Sliding Mode Control to Electro-Hydraulic Systems." *ASME 2014 12th Biennial Conference on Engineering Systems Design and Analysis*. 2014. American Society of Mechanical Engineers Digital Collection. DOI 10.1115/ESDA2014-20470.

[14] Schmidt, Lasse, Andersen, Torben O., Pedersen, Henrik C. and Bech, Michael M. "2-SMC of Electro-Hydraulic Drives Using the Twisting Algorithm." *Applied Mechanics and Materials* Vol. 233 (2012): pp. 131–134. DOI 10.4028/www.scientific.net/AMM.233.131.

[15] "Performance of Hydrostatic Machines - Extensive Measurement Report." Technical report no. INNAS BV. 2020.

[16] Li, Huaizhong, Gong, Z., Lin, W. and Lippa, T. "Motion Profile Planning for Reduced Jerk and Vibration Residuals." 2007.

[17] Lee, An Yong, Jang, Giho and Choi, Youngjin. "Infinitely Differentiable and Continuous Trajectory Planning for Mobile Robot Control." *2013 10th International Conference on Ubiquitous Robots and Ambient Intelligence (URAI)*: pp. 357–361. 2013. DOI 10.1109/URAI.2013.6677386.

[18] Hertz, Rasmus A, Christensen, Jesper K, Therkelsen, Ole, Kristiansen, Søren, Helver, Christian-Emil, Hansson, Frederik A and Schmidt, Lasse. "A Novel Approach to Control Switchover Between Injection and Holding Phase for a Hydraulic Injection Moulding Machine." *ANTEC23*. 2023. Denver.

[19] Zheng, Danian and Alleyne, Andrew. "Modeling and Control of an Electro-hydraulic Injection Molding Machine With Smoothed Fill-to-Pack Transition*." *Journal of Manufacturing Science and Engineering* Vol. 125 No. 1 (2003): pp. 154–163. DOI 10.1115/1.1540126.

[20] Havlicsek, H. and Alleyne, A. "Nonlinear Control of an Electrohydraulic Injection Molding Machine via Iterative Adaptive Learning." *IEEE/ASME Transactions on Mechatronics* Vol. 4 No. 3 (1999): pp. 312–323. DOI 10.1109/3516.789689.

[21] Graebe, S.F. and Ahlen, A.L.B. "Dynamic Transfer among Alternative Controllers and Its Relation to Antiwindup Controller Design." *IEEE Transactions on Control Systems Technology* Vol. 4 No. 1 (1996): pp. 92–99. DOI 10.1109/87.481772.

[22] Zheng, Danian and Alleyne, A. "Learning Control of an Electro-Hydraulic Injection Molding Machine with Smoothed Fill-to-Pack Transition." *Proceedings of the 2000 American Control Conference. ACC (IEEE Cat. No.00CH36334)*, Vol. 4: pp. 2558–2562 vol.4. 2000. DOI 10.1109/ACC.2000.878669.

[23] Huang, S.-J. and Lee, T.-H. "Application of Neural Networks in Injection Moulding Process Control." *The International Journal of Advanced Manufacturing Technology* Vol. 21 No. 12 (2003): pp. 956–964. DOI 10.1007/s00170-002-1417-9.

[24] Lin, Jeen and Lian, Ruey-Jing. "Self-Organizing Fuzzy Controller for Injection Molding Machines." *Journal of Process Control* Vol. 20 No. 5 (2010): pp. 585–595. DOI 10.1016/j.jprocont.2010.02.010.

[25] Froehlich, Christoph, Kemmetmüller, Wolfgang and Kugi, Andreas. "Model-Predictive Control of Servo-Pump Driven Injection Molding Machines." *IEEE Transactions on Control Systems Technology* Vol. 28 No. 5 (2020): pp. 1665–1680. DOI 10.1109/TCST.2019.2918993.